Structural and thermodynamic properties of diamond: A path-integral Monte Carlo study

Carlos P. Herrero and Rafael Ramírez
Instituto de Ciencia de Materiales, Consejo Superior de Investigaciones Científicas (C.S.I.C.), Campus de Cantoblanco, 28049 Madrid, Spain
(Received 23 June 2000; published 11 December 2000)

Path-integral Monte Carlo simulations in the isothermal-isobaric ensemble have been carried out to study structural and thermodynamic properties of diamond, as a function of temperature and hydrostatic pressure. Atomic nuclei were treated as quantum particles interacting through a Tersoff-type potential. The obtained lattice parameter, heat capacity, thermal expansion coefficient, and bulk modulus show an overall agreement with the experimental data. The importance of anharmonicity and quantum effects on the properties derived from the quantum simulations has been assessed by comparison with results obtained in classical simulations with the same interatomic potential, as well as with those derived from a quasiharmonic approximation. An increase in the lattice parameter by 1.7×10^{-2} Å and a decrease in the bulk modulus by about 5% is found at low temperatures, as a consequence of the zero-point motion of the C atoms.

DOI: 10.1103/PhysRevB.63.024103 PACS number(s): 65.40.−b, 65.40.De, 81.05.Uw

I. INTRODUCTION

Due to the interest of the solid phases of carbon in science and technology, many properties of its crystalline and amorphous phases have been studied by theoretical techniques, including *ab initio* methods,[1–7] as well as Monte Carlo[8–11] and molecular dynamics (MD) simulations.[12–14] In particular, the high-pressure properties of diamond are of enormous interest due to the importance of the diamond anvil cell in high-pressure physics.[15,16]

Ab initio methods such as the density-functional theory accurately predict several structural and dynamical properties of solids. For diamond, in particular, the lattice parameter, bulk modulus, and phonon-dispersion curves have been calculated by several authors.[1,4,7,17] Quantitative calculations of phenomena associated to the anharmonicity of the interatomic potential cannot, however, be carried out with such a degree of accuracy. Some progress in this line has been made in the last decade by combining *ab initio* electronic-structure calculations with the quasiharmonic approximation (QHA).[6,17–19] However, the validity range of these kinds of calculations is not clear, in particular for situations in which the anharmonicity cannot be treated as a small perturbation on the harmonic solid, which happens at high temperatures (e.g., thermal expansion coefficient).

A different approach to studying finite-temperature properties of condensed-matter systems is based on Monte Carlo (MC) or MD simulations. A basic point in these simulations is the model assumed for the microscopic interaction between atoms in the material. From a computational point of view, a feasible approach is based on the use of phenomenological potentials that describe the potential energy of the system as a function of the nuclear coordinates. Nevertheless, independently of the complexity of the approach employed to describe the interatomic interaction, it is interesting to study finite-temperature properties by methods that explicitly treat the quantum character of the nuclei. This is especially important for those properties that depend directly on the anharmonicity of the interaction potential (e.g., thermal expansion, isotopic effects). In this context, the Feynman path-integral (PI) approach to quantum statistical mechanics is a convenient method to study finite-temperature properties of quantum systems. The combination of Monte Carlo (MC) simulations with path integrals (the so-called PI MC method) is now a well-established method to study many-body problems in condensed matter.[20,21]

PI MC investigations on structural and dynamical properties of diamond-type semiconductors, such as silicon[22,23] and germanium,[24] have been already carried out. Since the carbon mass is smaller than that of Si and Ge, one expects that quantum effects associated to the anharmonicity of the interatomic potential will be more important in diamond than in the previously studied semiconductors. Classical simulations of solid phases of carbon have been carried out by using empirical interatomic potentials, such as that developed by Tersoff.[8,9] This potential was employed to study diamond and amorphous carbon,[8] as well as crystalline silicon,[25] C-Si and Si-Ge systems.[26] Further applications of this interatomic potential include Monte Carlo simulations of amorphous silicon carbide.[27] In the context of PI MC simulations, the Tersoff potential has been used previously to study the quantum delocalization of C nuclei in fullerenes.[28]

An alternative to the use of empirical potentials in materials simulations consists of deriving the system energy by standard electronic structure methods, as in the Car-Parrinello approach.[29] Such first-principles MD simulations have been carried out to study amorphization transitions and laser melting in diamond-type semiconductors.[30,31] Although the original version of this method considered the atomic nuclei as particles evolving in time according to the laws of classical physics, new approaches that take into account the quantum character of both electrons and nuclei have appeared in recent years. Thus, *ab initio* path-integral MD simulations have become feasible for small molecules,[32] and they begin now to be applied to condensed-matter problems.[33] These techniques constitute a promising tool to study, in the near future, the influence of anharmonic effects in solids.

In the present work, we report on results for several equilibrium properties of diamond, as derived from PI MC simu-

lations in the isothermal-isobaric (NPT) ensemble. The C atoms were treated as quantum particles interacting through an effective Tersoff-type potential. Furthermore, the simulation results have been analyzed by comparison with those yielded by a quasiharmonic approximation with the same interatomic potential. This study has been performed in a temperature range between 50 and 3000 K, and for hydrostatic pressures up to 6000 kbar.

The paper is organized as follows. In Sec. II we describe briefly the computational method and give some technical details. In Sec. III we present and discuss the results of our MC simulations, which are given in different subsections dealing with the internal energy, heat capacity, bulk modulus, crystal volume, and thermal expansion. The paper closes with a summary (Sec. IV).

II. COMPUTATIONAL METHOD

In the path-integral formulation of statistical mechanics (i.e., at finite temperatures), the partition function of a quantum system is evaluated through a discretization of the density matrix along cyclic paths, composed of a finite number L (Trotter number) of ''imaginary-time'' steps.[35] In the numerical simulations, each quantum particle is described by a set of L ''beads,'' forming a cyclic chain. Thus, the implementation of the PI MC method is based on an isomorphism between the actual quantum system and a classical one, obtained by replacing each quantum particle (here, atomic nucleus) by a chain of L classical particles (beads). This means that a simulation of N quantum particles is equivalent to one of NL classical particles. This isomorphism is exact in the limit $L\rightarrow\infty$, but convergence of the interesting quantities is obtained for relatively low L values. Extensive descriptions of this computational method can be found elsewhere.[20,21,23]

Equilibrium properties of diamond have been calculated by PI MC simulations, in the isothermal-isobaric ensemble. These simulations have been performed on a $2\times2\times2$ supercell of the diamond face-centered-cubic cell including 64 C atoms, with periodic boundary conditions. We have checked that using larger supercells does not change appreciably any of the results presented below. In particular, we have carried out PI MC simulations on a $3\times3\times3$ supercell at three different temperatures, and found that the results coincide (within error bars) with those obtained for the $2\times2\times2$ supercell. The C nuclei were treated as quantum particles interacting through a Tersoff-type potential.[8,25] We have used the original parameters given by Tersoff,[8] with the exception of $A=1387.3$ eV and $B=348.3$ eV, which give for the lattice parameter derived from PI MC simulations an agreement with experimental results, better than the original A and B parameters in Ref. 8. For given temperature and pressure, we generated in our PI MC simulations 3×10^4 quantum paths per atom for system equilibration, and 5×10^5 paths per atom for the calculation of ensemble average properties. More details on the actual application of this method are given in Ref. 23.

To keep a constant precision for the results at different temperatures, we have considered a Trotter number L that scales as the inverse temperature. In fact, we have taken L as the integer number closest to $\hbar\omega_c/(k_BT)$, with $\omega_c\sim3\omega_D$ (ω_D, Debye frequency of diamond), which is enough for convergence of the results. This means: $\omega_c=4200$ cm^{-1}, which translates into a product $LT=6000$ K, i.e., $L=20$ at $T=300$ K. We have checked the convergence with the Trotter number of several quantities derived from the PI MC simulations. In Fig. 1 we show the convergence of the equilibrium lattice parameter of diamond, as a function of L. The results presented in this figure correspond to atmospheric pressure and two different temperatures: $T=400$ and 1000 K. The resulting lattice parameter increases with rising L, starting from the classical value corresponding to each temperature (indicated in the figure by black symbols), which is obtained for $L=1$. For $LT\sim6000$ K, the lattice parameter converges to a plateau (the quantum value) for each temperature. In general, the results of the PI MC simulations converge at high temperatures ($T>\Theta_D$) to those corresponding to classical simulations with $L=1$. At lower temperatures, the CPU time required to carry out the quantum simulations increases as $1/T$, proportional to the Trotter number L. This means, for example, that at $T=300$ K our PI MC simulations require a CPU time 20 times longer than that corresponding to a classical simulation with the same interatomic potential.

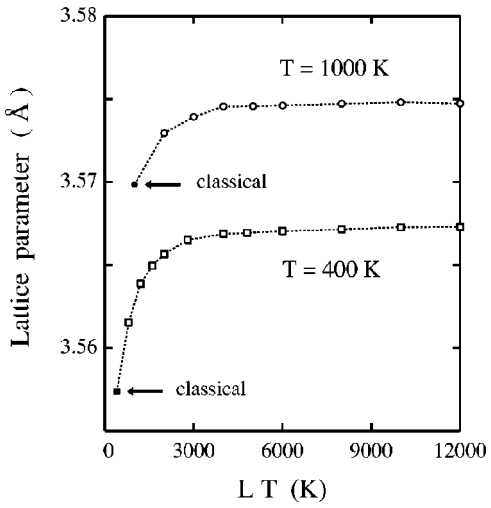

FIG. 1. Lattice parameter of diamond, as derived from PI MC simulations at $T=400$ and 1000 K as a function of the product LT, with L the Trotter number. Black symbols indicate the results of classical MC simulations ($L=1$). Dotted lines are guides to the eye.

For simulations in the isothermal-isobaric ensemble, the volume of the simulation cell, Ω, is allowed to change. If we call $V=\langle\Omega\rangle$, then the mean-square fluctuation in the volume, $\Delta^2=\langle\Omega^2\rangle-V^2$, is given by

$$\Delta^2=\frac{V}{B}k_BT, \tag{1}$$

where $B=-V(\partial P/\partial V)_T$ is the isothermal bulk modulus of the material. In Fig. 2 we present the normalized fluctuations $(\Delta/V)^2$, as obtained from our PI MC simulations at different

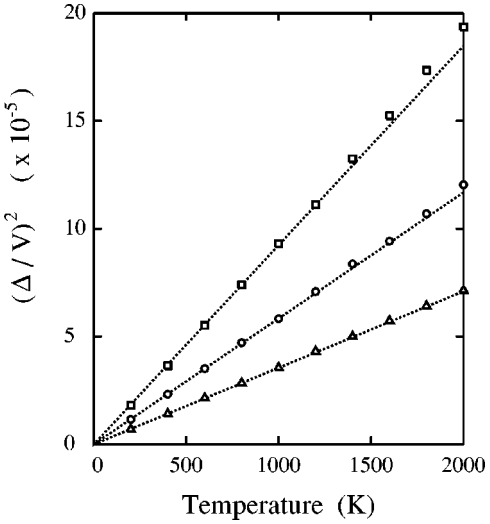

FIG. 2. Mean-square fluctuations in the volume of the simulation cell, $\Delta^2=\langle\Omega^2\rangle-\langle\Omega\rangle^2$, as derived from path-integral Monte Carlo simulations at different hydrostatic pressures. These fluctuations are shown normalized by $V^2=\langle\Omega\rangle^2$. Squares, $P=1$ atm; circles, 1000 kbar; triangles, 4000 kbar. Dotted lines are linear fits to the low-temperature results.

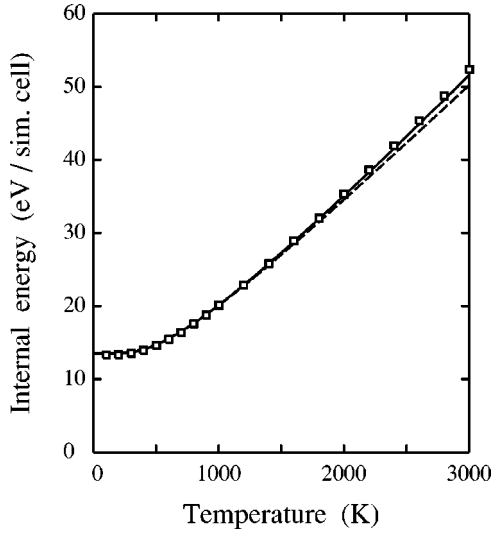

FIG. 3. Temperature dependence of the internal energy E per simulation cell. Open squares: results of PI MC simulations; continuous line: quasiharmonic approximation; dashed line: harmonic approximation with the volume and phonon frequencies at $T=0$. The zero of energy corresponds to the classical limit at $T=0$.

temperatures, and for three hydrostatic pressures (squares, 1 atm; circles, 1000 kbar; triangles, 4000 kbar). Dotted lines are linear fits to the low-temperature ($T\leqslant 1000$ K) MC data. The fluctuations in the cell volume decrease as pressure rises, due to an increase in the bulk modulus of the material (see below). At $T=2000$ K and $P=1$ atm, the relative fluctuation in the simulation-cell volume, Δ/V, amounts to 0.014. As expected from Eq. (1), Δ^2 increases approximately linearly with the temperature, with a slope proportional to B^{-1}. Nevertheless, deviations from linearity are evident in the results shown in Fig. 2, as a consequence of changes in B and V with the temperature, especially at low hydrostatic pressures.

In the following section, results of the PI MC simulations will be compared with those derived from a QHA. This approximation is based on a renormalization of the phonon frequencies with volume, and for a given volume the solid is assumed to be harmonic.[34,36] This volume dependence of phonon frequencies is usually described by a mode-dependent Grüneisen parameter[36] $\gamma_n(\mathbf{q})=-\partial\ln\omega_n(\mathbf{q})/\partial\ln V$, where $\omega_n(\mathbf{q})$ are the frequencies of the nth mode in the crystal. For small volume changes this parameter can be assumed to be constant for each mode. For the QHA calculations presented here, we have employed the same supercell as for the PI MC simulations, i.e., a $2\times2\times2$ supercell with periodic boundary conditions. This means that only the $\mathbf{q}=0$ modes in the Brillouin zone of the supercell are included in the calculation, as modes with $\mathbf{q}\neq0$ violate the periodic boundary conditions. Then, the total number of vibrational modes in the QHA is 189, i.e., three times the number of C atoms in the supercell minus three translational degrees of freedom. The Grüneisen parameters $\gamma_n(\mathbf{q})$ were obtained by numerical differentiation of the vibrational frequencies $\omega_n(\mathbf{q})$ calculated by diagonalization of the dynamical matrix corresponding to two supercells, whose lattice parameter deviated by 5×10^{-4} Å from the equilibrium value. For each temperature, we calculated the free energy as a function of volume, with the corresponding renormalized phonon frequencies. The lattice parameter was changed in steps of 10^{-4} Å, and from the free-energy curve we obtained the equilibrium volume as a function of pressure.

III. RESULTS AND DISCUSSION

A. Internal energy

For given volume and temperature, the internal energy of the crystal, $E(V,T)$, can be written as

$$E(V,T)=E_0+E_S(V)+E_{vib}(V,T), \tag{2}$$

where E_0 is the minimum potential energy for the (classical) crystal at $T=0$, $E_S(V)$ is the elastic energy, and $E_{vib}(V,T)$ is the vibrational energy. With the parameters employed here for the Tersoff potential, we find $E_0=-481.302$ eV per simulation cell (64 atoms), which corresponds to a (classical) lattice parameter $a_C(0)=3.5493$ Å, to be compared with $a_C(0)=3.5656$ Å obtained with the original Tersoff potential.[8] That value for E_0 translates into a cohesive energy of 7.52 eV per atom.

In Fig. 3 we plot the temperature dependence of the internal energy (kinetic plus potential) obtained in the PI MC simulations at atmospheric pressure (open squares). In this figure we have taken as zero the minimum of potential energy (E_0). The solid line represents the internal energy in a QHA approximation with the same interatomic potential. For comparison, we also present the result of a totally harmonic approximation (crystal volume independent of temperature) in the same temperature region (dashed line). The harmonic approximation may be viewed as a limiting case of the QHA, when the Grüneisen parameters are set equal to zero. The

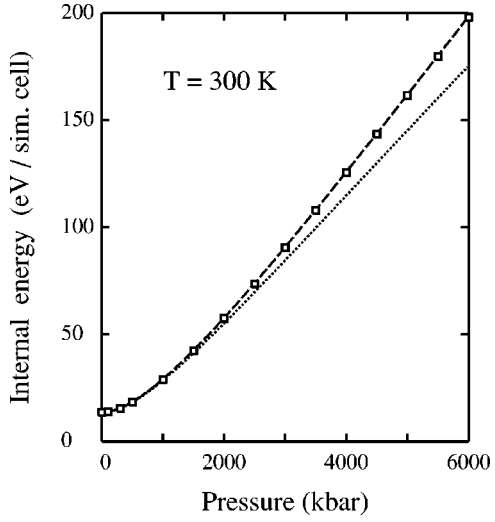

FIG. 4. Pressure dependence of the internal energy, E, of diamond at $T=300$ K. Open squares are results derived from PI MC simulations. Error bars are less than the symbol size. The dashed line corresponds to the quasiharmonic approximation with the Tersoff-type potential. The dotted line is the prediction of Murnaghan's law [see Eq. (3)] with $B_0=4.18$ Mbar and $B_0'=3.97$.

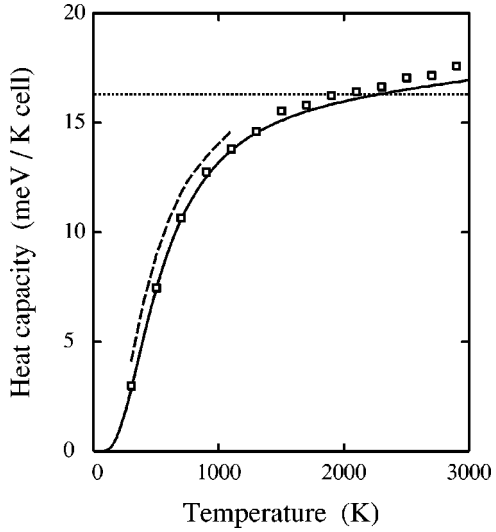

FIG. 5. Temperature dependence of the heat capacity C_P of diamond at $P=1$ atm. Open squares are results derived from PI MC simulations by numerical differentiation of the enthalpy. The solid line is the quasiharmonic prediction. The dashed line shows the experimental temperature dependence of C_P (Refs. 41 and 42). The dotted line indicates the C_P value corresponding to the classical harmonic limit (Dulong-Petit's law).

energy values derived in the QHA follow closely those found in the PI MC simulations, although the simulation results are slightly larger at temperatures higher than 2000 K. At 3000 K, this difference amounts to 0.69 eV per simulation cell. At 300 K, the internal energy found in the simulations is -467.76 eV, which corresponds to a cohesive energy of 7.31 eV per atom, close to the experimental value of 7.36 eV.[37] The internal energy shown in Fig. 3 corresponds basically to the vibrational energy $E_{vib}(V,T)$. For $T\rightarrow 0$ (zero-point motion) this energy amounts to 13.31 eV per simulation cell (0.21 eV per atom). The elastic energy $E_S(V)$ represents a small part of the internal energy, and amounts to 0.10 and 1.43 eV per cell at 300 and 3000 K, respectively.

In Fig. 4 we present the pressure dependence of the internal energy at $T=300$ K. Open squares represent data obtained from our PI MC simulations, whereas the dashed line is the result of the QHA. Differences between results of both kinds of calculations are less than 0.5 eV in the whole pressure range considered here, and are not detectable at the scale of the figure. The vibrational energy at 300 K increases from 13.4 eV per simulation cell at $P=1$ atm, to 17.2 and 20.8 eV at $P=2000$ and 6000 kbar, respectively. Thus, the largest contribution to the internal energy, $E(V,T)-E_0$, at pressures $P\gtrsim 2000$ kbar comes from the elastic energy $E_S(V)$.

For comparison with our results, we also present in Fig. 4 the pressure dependence of the zero-temperature internal energy predicted by the Murnaghan's equation of state:[38]

$$E(V,0)=\frac{B_0V}{B_0'}\left[\frac{(V_0/V)^{B_0'}}{B_0'-1}+1\right]+C, \qquad (3)$$

where $C=E(V_0,0)-B_0V_0/(B_0'-1)$ is a constant and the subindex zero indicates $P=0$. This equation has been employed in the literature to fit the volume dependence of calculated energies.[17,39,40] It was derived under the assumption that the bulk modulus B of the material is linear with the pressure: $B(P)=B_0+B_0'P$, and in our case gives good agreement with the internal energy derived from MC and QHA at $P\lesssim 2000$ kbar. At higher hydrostatic pressures the error in the linear assumption grows rapidly (see below), and the dashed line lies clearly below the simulation results. Apart from this difference at high pressures, Eq. (3) is strictly valid only at $T=0$, but one expects that it will be a good approximation at temperatures where the entropy contribution to the free energy is negligible versus the internal energy. This seems to be the case here for $T=300$ K, a temperature several times lower than the Debye temperature of diamond.

B. Heat capacity

In Fig. 5 we show the heat capacity C_P obtained from the MC simulations at $P=1$ atm as a numerical derivative of the enthalpy, $H=E+PV$, with respect to the temperature. The solid line corresponds to a QHA with the Tersoff-type potential. For comparison, we also give the prediction of a classical harmonic approximation (dotted line). Results of the QHA coincide with those derived from the MC simulations at $T<1000$ K. At higher temperatures, the QHA predicts C_P values smaller than the simulation results. This could be expected from the trend of the internal energy vs the temperature, as at high T the MC simulations give energy values larger than the QHA (see Fig. 3). The experimental results[41,42] are given as a dashed line. The calculated line (MC and QHA) is about 70 K displaced to high temperatures, as compared with the actual heat capacity of diamond.

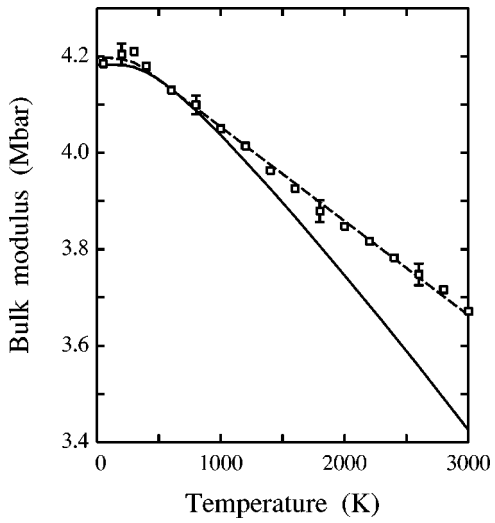

FIG. 6. Temperature dependence of the bulk modulus of diamond, as derived from PI MC simulations (open squares). A continuous line shows the result of a QHA. The dashed line through the data points is a guide to the eye.

This is basically due to a shift toward higher frequencies of the optical phonons calculated with the Tersoff potential.[8]

At low temperatures, finite size effects are expected to be observed in the heat capacity derived from PI MC simulations. Due to the small dimensions of the simulation cell, long-wavelength acoustic phonons (close to the center of the Brillouin zone), which are expected to contribute largely to the heat capacity at low T, are truncated. This causes the appearance of an effective energy gap for vibrational excitations in the simulated solid, that is not present in the actual material. In this manner, Müser *et al.*[43] carried out detailed PI MC simulations of Lennard-Jones solid systems, and discussed the effect of size scaling on the specific heat of solid argon at low temperatures. In our simulations for diamond, this effect causes a decrease in the heat capacity derived from the MC simulations at temperatures lower than 300 K.

C. Bulk modulus

The isothermal bulk modulus B is related with the mean-square fluctuations in the volume V of the simulation cell by Eq. (1). By using this relation, we have calculated the bulk modulus as a function of temperature and pressure from the volume fluctuations Δ^2 obtained in the MC simulations. In Fig. 6 we present the temperature dependence of B up to 3000 K and at atmospheric pressure. Open squares are results derived from the simulations, and the dashed line through the data points is a guide to the eye. The continuous line shows the result of a QHA with our Tersoff potential. The results of the QHA and MC coincide (within error bars of the MC data) at low temperatures ($T<1000$ K). At higher T, as anharmonicity becomes more relevant, the bulk modulus predicted by the QHA is lower than that found in the MC simulations, and at 3000 K this difference is about 7% of the MC value. The calculated bulk modulus is rather constant up to 300 K, and at higher temperatures it decreases roughly linearly. At 1000 K and 3000 K, the MC simulations give a decrease of about 3% and 12% with respect to the $T=0$ value, respectively.

We have also calculated the bulk modulus at $T=0$ from the elastic energy $E_S(V)$ obtained for classical nuclei, as $B_C=V(\partial^2 E_S(V)/\partial V^2)$. This yields $B_C=4.37$ Mbar, a value clearly higher than that found when zero-point motion is considered ($B=4.18$ Mbar). The bulk modulus with the original parameters of Tersoff, as obtained from the elastic constants given in Ref. 8, is $B=4.43$ Mbar. This value is very close to the bulk modulus found from experiments at room temperature ($B=4.42$ Mbar from Brillouin scattering[44] and 4.43 Mbar from ultrasonics data[45]), that the effective interaction potential tried to reproduce. However, we see that consideration of quantum effects changes the calculated low-temperature bulk modulus by $\delta B=-0.19$ Mbar. This applies also to *ab initio* calculations, in which the bulk modulus is obtained from a second derivative of the internal energy (at $T=0$ and with classical nuclei) respect to the volume. With this in mind, the values calculated with these methods,[1,3,17,46] although close to the experimental value of B at room temperature, could not be considered more accurate than $\sim\pm 0.2$ Mbar (i.e., $\sim 5\%$), as usually they do not take into account the influence of quantum effects. In this line, Karch *et al.*[19] have calculated the contribution of quantum fluctuations to the bulk modulus of diamond, by density-functional perturbation theory, and found $\delta B=-0.12$ Mbar. The larger value of $\delta B=-0.19$ Mbar obtained in our simulations can be due to the neglect of higher-order terms in the perturbative expansion of Ref. 19 and/or to differences in the interatomic potentials employed in both kinds of calculations. No answer to this question is available at this point.

This trend of quantum effects to reduce the bulk modulus seems to be general in solids. Nevertheless, the influence of zero-point motion on B will depend on the atomic mass, and for growing mass this effect is expected to become less relevant. Thus, for silicon a decrease of ~ 0.03 Mbar was found at low temperatures (about 3% of the actual B value), when quantum effects were considered.[23] For diamond, it is worthwhile emphasizing that the B values obtained in classical simulations are closer to the experimental data than those derived from the quantum simulations. This is a consequence of the fact that the employed potential was obtained by using classical calculations to fit the actual bulk modulus. It is expected that the use of potentials derived from first-principles calculations in PI MC simulations should fix this problem.

In Fig. 7 we present the pressure dependence of the bulk modulus of diamond at 300 K. Symbols represent values derived from the PI MC simulations; squares correspond to values obtained by using Eq. (1), and circles denote those found by numerical differentiation of the pressure-volume curve (see below). Both procedures give results agreeing with each other (within error bars), and also with the prediction of our QHA (continuous line). The dashed line corresponds to the linear relation $B=B_0+B_0'P$ with $B_0=4.18$ Mbar and $B_0'=3.97$, obtained with the Tersoff-type potential employed here. This value for the pressure deriva-

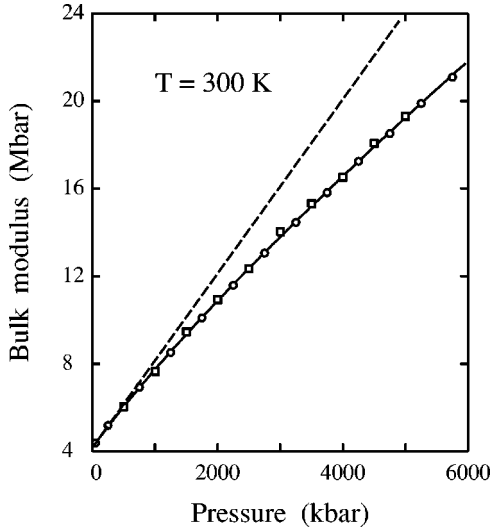

FIG. 7. Pressure dependence of the bulk modulus of diamond at $T=300$ K. Symbols indicate values derived from PI MC simulations by two different methods: by numerical differentiation of the pressure-volume results (circles), and from the volume fluctuations by using Eq. (1) (squares). Error bars are less than the circle size and of the order of the square size. The dashed line corresponds to $B=B_0+B_0'P$, with $B_0=4.18$ Mbar and $B_0'=3.97$.

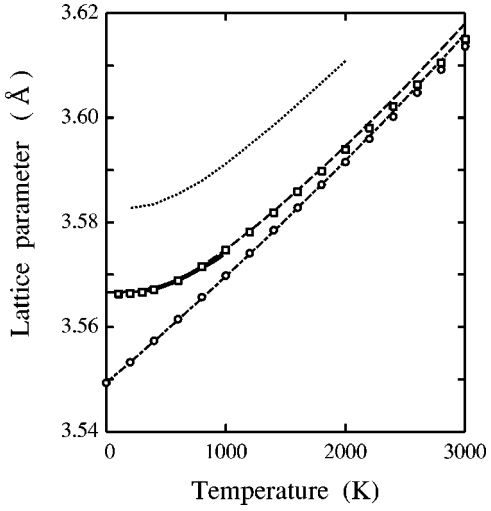

FIG. 8. Temperature dependence of the lattice parameter a. The simulation results were derived at $P=1$ atm within the quantum PI approach (squares) and in the classical limit (circles). Dashed and dashed-dotted lines were obtained in a quantum and classical quasiharmonic approach, respectively. The experimental results (Ref. 41) are given as a bold line. The dotted line was obtained from PI MC simulations with the original Tersoff potential given in Ref. 8.

tive B_0' is larger than those calculated by functional-density-theory calculations, which range from 3.24 in Ref. 46 to 3.5 in Refs. 4,17. From the pressure derivatives of the elastic moduli, measured by McSkimin and Andreatch[45] at room temperature, one finds $B_0'=4.0\pm0.7$. At the scale of Fig. 7, B departs appreciably from the linear behavior at pressures larger than 1000 kbar. At 3000 and 4000 kbar the change in B due to higher powers of P amounts to 14 and 18%, respectively.

D. Crystal volume

The temperature dependence of the equilibrium lattice parameter, a, obtained in our MC simulations at atmospheric pressure is displayed in Fig. 8. Results of the quantum simulations with the Tersoff-type potential are in good agreement with values derived from diffraction experiments[41] (bold line). For comparison, a dotted line shows the results obtained from PI MC simulations with the original Tersoff potential.[8] It lies about 1.7×10^{-2} Å above the open squares in the entire temperature range from 0 to 2000 K. The main reason for this shift in the lattice parameter, a, is that Tersoff parameterized his potential by fitting the volume expected in the $T=0$ classical limit to the experimental volume at $T=300$ K. The dashed line displays the lattice parameter obtained in a (quantum) QHA with the Tersoff-type potential employed here. This approximation yields values for the lattice parameter close to those derived from the MC simulations. However, for $T>2000$ K there appears a systematic trend of the simulation results to lie lower than the QHA values. At 3000 K, this difference amounts to 3.1×10^{-3} Å.

In the zero-temperature limit we find from the MC simulations $a(0)=3.5663(\pm10^{-4})$ Å, a value slightly lower than that found in the QHA [$a(0)=3.5667$ Å]. Taking into account that in the classical limit at $T=0$ we have $a_C(0)=3.5493$ Å, the lattice expansion due to zero-point motion and anharmonicity amounts to $\delta a=1.7\times10^{-2}$ Å. This difference is much larger than the precision currently achieved in the determination of cell parameters from x-ray diffraction techniques.[47–49] This zero-point lattice expansion is equivalent to the effect of a hydrostatic pressure of -61 kbar, and is larger than that found in earlier simulations of diamond-type materials. For silicon and germanium, using PI MC simulations with Stillinger-Weber-type potentials, it was found $\delta a=7\times10^{-3}$ Å and 6×10^{-3} Å, respectively.[23,24,50] At room temperature, the PI MC simulations of diamond give $a=3.5666$ Å, vs the experimental value $a=3.5668$ Å.[41] The lattice expansion from $T=0$ to 300 K is small, and amounts to $\sim3\times10^{-4}$ Å, about 6 times smaller than the zero-point expansion. This zero-point expansion is nearly the same as the thermal expansion from 0 to 1500 K. Similar quantum effects on the lattice parameter of Lennard-Jones solids have been studied earlier by PI MC.[43]

For comparison with the results of the quantum simulations, we have also displayed in Fig. 8 the temperature dependence of a_C in the classical limit with the present Tersoff-type potential. Open circles are the results of classical MC simulations and the dashed-dotted line displays those of a classical QHA (the vibrational modes are considered as classical harmonic oscillators with frequencies renormalized for each volume). As expected, both kinds of classical calculations yield at $T=0$ the lattice parameter corresponding to the minimum potential energy of the (classical) crystal. At high temperatures, each one approaches its corresponding quantum calculation.

In Fig. 9 we display the pressure dependence of the crystal volume at 300 K. Open squares are the results of the PI

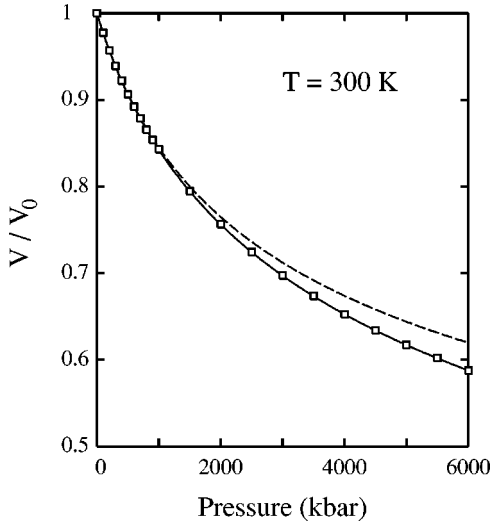

FIG. 9. Pressure-volume equation-of-state for diamond at 300 K. Open squares are results of PI MC. The continuous line was obtained in the quasiharmonic approximation. The dashed line corresponds to Murnaghan's law [see Eq. (4)] with $B_0=4.18$ Mbar and $B_0'=3.97$. V_0 is the volume at zero pressure.

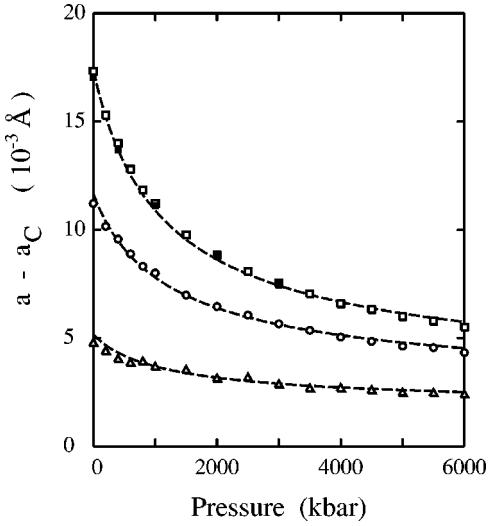

FIG. 10. Difference $a-a_C$ between the lattice parameter of a (quantum) diamond crystal and that corresponding to the classical limit. Symbols represent data points derived from MC simulations at different temperatures: triangles, $T=1000$ K; circles, $T=300$ K; open and black squares, low-temperature limit (see text for details). Dashed lines indicate results obtained from a QHA with the same Tersoff-type potential employed in the simulations.

MC simulations, and the solid line corresponds to the QHA. Both results coincide in the whole pressure range considered, up to 6000 kbar. This indicates that the QHA is accurate, even for such large hydrostatic pressures. The dashed line shows the volume-pressure relation derived from Murnaghan's equation of state:[38]

$$P=\frac{B_0}{B_0'}\left[\left(\frac{V_0}{V}\right)^{B_0'}-1\right], \tag{4}$$

in which we have introduced the B_0 and B_0' values given above. For pressures larger than $\sim$1000 kbar, this approximation predicts volumes larger than those found in the MC simulations, since the bulk modulus given by Murnaghan's law is also larger (see Fig. 7). However, this approach gives a good approximation to the results of the quantum simulations for pressures lower than 1000 kbar.

It is interesting to analyze the influence of quantum effects on the lattice parameter, as a function of the applied pressure. This is presented in Fig. 10, where we show the difference $a-a_C$ between the lattice parameters corresponding to the quantum and classical approaches. Different symbols correspond to results of MC simulations (quantum and classical), and dashed lines to those of the QHA at different temperatures: 1000 K (triangles), 300 K (circles), and zero-temperature limit (open and black squares). Since PI MC simulations cannot be carried out strictly at $T=0$, squares correspond to the difference $a-a_C$ with a_C obtained from classical MC simulations at $T=0$, but with a calculated at temperatures low enough to be close to $a(0)$: 100 K (black squares) and 300 K (open squares). The proximity of both kinds of symbols for a given pressure indicates the convergence of the results. The QHA provides a very good description of the difference $a-a_C$ in the whole pressure range investigated here. This approximation is expected to be less accurate for high temperatures, as anharmonic effects not included in the QHA should become more relevant. However, even for $T=1000$ K, the QHA gives results for $a-a_C$ very close to the PI MC simulations.

The decrease in the difference $a-a_C$ as pressure rises is due basically to the increase in bulk modulus with pressure. This can be understood by expressing the lattice parameter as a function of the Grüneisen parameters in a QHA.[36,51] For a given pressure, one can expand the lattice parameter $a(T,P)$ to first order in $\gamma_n(\mathbf{q})$ (for small volume changes as a function of T), as

$$a(T,P)=a_C(0,P)+\frac{1}{3B(P)a_C^2(0,P)}\sum_{n,\mathbf{q}}\gamma_n(\mathbf{q})E_n(\mathbf{q},T), \tag{5}$$

where

$$E_n(\mathbf{q},T)=\frac{1}{2}\hbar\omega_n(\mathbf{q})\coth\left(\frac{\hbar\omega_n(\mathbf{q})}{2k_BT}\right). \tag{6}$$

Here, $B(P)$ is the bulk modulus at zero temperature and pressure P, and $a_C(0,P)$ is the zero-temperature limit of the classical lattice parameter. In this approximation, one finds

$$a(T,P)-a_C(T,P)=\frac{1}{3B(P)a_C^2(0,P)}\times\sum_{n,\mathbf{q}}\gamma_n(\mathbf{q})[E_n(\mathbf{q},T)-k_BT], \tag{7}$$

indicating that, for given T and P, the difference $a-a_C$ is, to first order in $\gamma_n(\mathbf{q})$, proportional to $B(P)^{-1}$. When pressure is modified, the relative changes in $a_C(0,P)$ [which appears

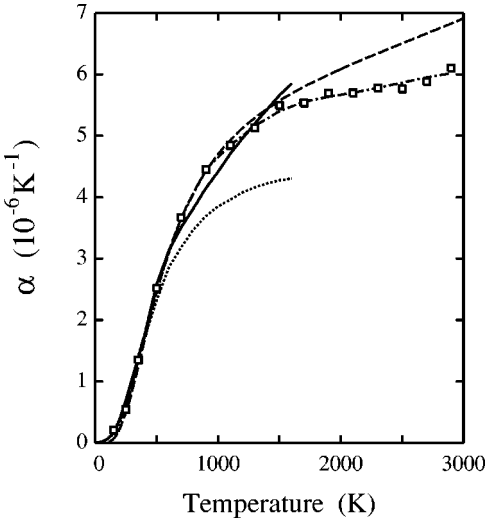

FIG. 11. Thermal expansion coefficient of diamond as a function of temperature at atmospheric pressure. Squares are results derived from PI MC simulations by numerical differentiation of the lattice parameter $a(T)$. The dashed line is the result of a QHA with the Tersoff-type potential employed here. The solid line shows the experimental results. (Ref. 52). The dashed-dotted line through the data points is a guide to the eye. The dotted line indicates results found by Pavone *et al.*[17] from density-functional-theory calculations in a QHA.

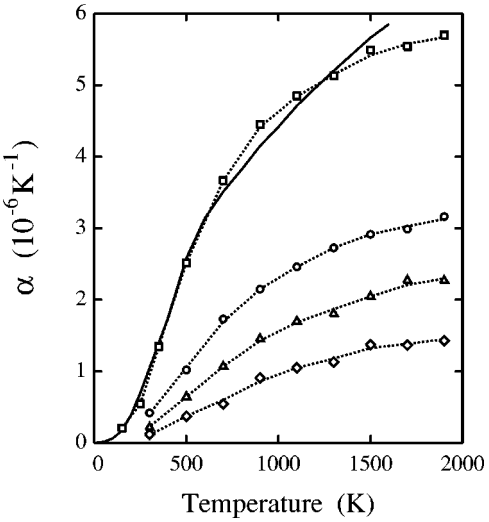

FIG. 12. Thermal expansion coefficient of diamond as a function of temperature at different pressures. Squares and the solid line are simulation results and experimental data at $P=1$ atm, as in Fig. 11. Other symbols correspond to results at several hydrostatic pressures: circles, 1000 kbar; triangles, 2000 kbar; diamonds, 4000 kbar. Dotted lines are guides to the eye.

in the denominator on the r.h.s. of Eq. (7)] are much smaller than those in $B(P)$. Thus, at any temperature, $a-a_C$ decreases as pressure is raised, since $B(P)$ becomes larger. This is basically the trend found in the more precise calculations (QHA and MC) shown in Fig. 10.

E. Thermal expansion

The linear coefficient of thermal expansion:

$$\alpha=\frac{1}{a}\left(\frac{\partial a}{\partial T}\right)_P, \tag{8}$$

has been obtained by numerical differentiation of the simulation results for $a(T)$ at atmospheric pressure. Values of α derived by this method (squares) are compared in Fig. 11 with experimental data for diamond[52] (bold line). The dashed-dotted line through the MC data is a guide to the eye. Results of the QHA are given by a dashed line. This line closely follows the results of the PI MC simulations up to $\sim$1000 K, and departs from them at higher T. At these temperatures, the thermal expansion coefficient derived from the QHA is larger than that obtianed from PI MC, as expected from the high-temperature results for $a(T)$ shown in Fig. 8. The dotted line in Fig. 11 shows results for $\alpha(T)$ derived by Pavone *et al.*[17] from density-functional theory calculations in a QHA. These theoretical results follow closely the experimental values for $T\lesssim 500$ K, but seem to saturate to a constant value $\alpha_{HT}\simeq 4.3\times 10^{-6}$ K^{-1} at high temperatures. Such a saturation is expected in calculations employing expansions like that given for $a(T)$ in Eq. (5), as in Ref. 17 [see also Ref. 18 for a similar calculation of $\alpha(T)$ for silicon]. In fact, from Eq. (5) the QHA gives for the thermal expansion coefficient [to first order in $\gamma_n(\mathbf{q})$]:

$$\alpha(T,P)=\frac{1}{3B(P)V(0,P)}\sum_{n,\mathbf{q}}\gamma_n(\mathbf{q})C_{V,n}(\mathbf{q},T), \tag{9}$$

with $C_{V,n}(\mathbf{q},T)=dE_n(\mathbf{q},T)/dT$. Then, in the high-temperature limit ($T>\Theta_D$), one has

$$\alpha(T,P)=\frac{k_B}{3B(P)V(0,P)}\sum_{n,\mathbf{q}}\gamma_n(\mathbf{q}), \tag{10}$$

and the thermal expansion coefficient should go to a constant. Since the experimental result indicates that α increases at high T (see Fig. 11), that approximation should fail at high T, irrespective of the interatomic potential employed in the calculations. When one considers the QHA, without the linearization assumed in Eq. (5), α does not saturate to a constant value at high T, as shown by our calculations (dashed line in Fig. 11).

Taking into a account the increase in bulk modulus as the pressure is raised, one expects that α will decrease [see Eq. (9)]. This is in fact found in our PI MC simulations, and shown in Fig. 12. In this figure, open squares and the solid line represent atmospheric-pressure results, as in Fig. 11. Results for α at different hydrostatic pressures are shown by different symbols: circles (1000 kbar), triangles (2000 kbar), and diamonds (4000 kbar). Dotted lines are guides to the eye. At 300 K, a hydrostatic pressure of 1000 kbar reduces α by about a factor of 2, and this factor is nearly unchanged from room temperature up to 2000 K. For higher pressures, a further reduction of α is found.

IV. SUMMARY

In this paper, we have studied the influence of quantum effects on structural and thermodynamic properties of diamond by PI MC simulations. These quantum effects are nontrivial in the presence of anharmonicity. For situations in which anharmonic effects can be treated perturbatively (i.e., low temperatures), the QHA gives a good description of the studied quantities, but this approximation becomes less accurate as temperature is raised. Quantum MC simulations with the path-integral method have allowed us to check the precision of the QHA approximation for diamond with an effective interaction potential. Results of this approximation for several properties of diamond at room temperature are very close to those found from PI MC simulations. This agreement is still valid at high pressures, of the order, and even larger, than those currently achieved in diamond anvil cells. At a microscopic scale, when pressure is increased the atoms are forced to move towards shorter interatomic distances, where the interaction potential is comparatively more repulsive. Then, the QHA is able to give a good description of the thermodynamic properties of the material for conditions in which those high-energy regions are visited. However, some differences between QHA and PI MC are found at temperatures higher than 1000 K, in particular for the bulk modulus, thermal expansion coefficient, and heat capacity. This is a consequence of the enhancement of anharmonic effects at high temperatures, for which the quasiharmonic approximation can be considered to give only qualitative trends.

We have shown that the zero-point lattice expansion (due to anharmonicity of the zero-point vibrational motion) is a nonnegligible effect. For diamond, this effect causes an increase in the lattice parameter of 0.017 Å (a relative change of 0.5%) and a decrease in the bulk modulus by 5%. Note that these values are of the same order of magnitude as the precision currently available by the best *ab initio* electronic structure methods. This means that, at least for materials with light atoms, further improvements in the treatment of the electronic structure cannot reduce the error bars in the calculation of structural observables, if the effects associated to the quantum nature of the atomic nuclei are not included in the calculations.

We finally note that, in spite of the limitations associated to employing empirical potentials originally optimized for classical simulations, a reasonable agreement has been found between PI MC and experimental results for several thermodynamic properties of diamond, as heat capacity and thermal expansion coefficient. For the heat capacity, we have obtained values lower than the experimental ones, due to the rigidity of the Tersoff potential, which gives a shift of the phonon frequencies to higher wave numbers. However, this rigidity does not seem to affect directly the calculated values for the lattice parameter and thermal expansion. It is expected that these limitations will be overcome in the near future by the use of *ab initio* PI MC simulations, where the interatomic interaction is derived from first-principles calculations.

ACKNOWLEDGMENTS

We thank T. López-Ciudad for critically reading the manuscript. This work was supported by CICYT (Spain) under Contract No. PB96-0874, and by the European Union through FEDER Project No. 1FD97-1358.

[1] M.L. Cohen, Phys. Rev. B **32**, 7988 (1985).
[2] M. Hanfland, K. Syassen, S. Fahy, S.G. Louie, and M.L. Cohen, Phys. Rev. B **31**, 6896 (1985).
[3] O.H. Nielsen, Phys. Rev. B **34**, 5808 (1986).
[4] S. Fahy, K.J. Chang, S.G. Louie, and M.L. Cohen, Phys. Rev. B **35**, 5856 (1987).
[5] J. Bernholc, A. Antonelli, T.M. Del Sole, Y. Bar-Yam, and S.T. Pantelides, Phys. Rev. Lett. **61**, 2689 (1988).
[6] P. Pavone and S. Baroni, Solid State Commun. **90**, 295 (1994).
[7] B.R. Wu and J. Xu, Phys. Rev. B **60**, 2964 (1999).
[8] J. Tersoff, Phys. Rev. Lett. **61**, 2879 (1988).
[9] J. Tersoff, Phys. Rev. B **44**, 12 039 (1991).
[10] J. Xing and H.L. Scott, Phys. Rev. B **48**, 4806 (1993).
[11] J.K. Walters, K.W.R. Gilkes, J.D. Wicks, and R.J. Newport, J. Phys.: Condens. Matter **9**, L457 (1997).
[12] D.W. Brenner, Phys. Rev. B **42**, 9458 (1990).
[13] G. Kopidakis, C.Z. Wang, C.M. Soukoulis, and K.M. Ho, J. Phys.: Condens. Matter **9**, 7071 (1997).
[14] S. Serra, G. Benedek, M. Facchinetti, and L. Miglio, Phys. Rev. B **57**, 5661 (1998).
[15] A. Jayaraman, Rev. Mod. Phys. **55**, 65 (1983).
[16] R.J. Hemley and N.W. Ashcroft, Phys. Today **51** (8), 26 (1998), and references therein.
[17] P. Pavone, K. Karch, O. Schütt, W. Windl, D. Strauch, P. Giannozzi, and S. Baroni, Phys. Rev. B **48**, 3156 (1993).
[18] S. Biernacki and M. Scheffler, Phys. Rev. Lett. **63**, 290 (1989).
[19] K. Karch, T. Dietrich, W. Windl, P. Pavone, A.P. Mayer, and D. Strauch, Phys. Rev. B **53**, 7259 (1996).
[20] M. J. Gillan, in *Computer Modelling of Fluids, Polymers, and Solids*, edited by C. R. A. Catlow, S. C. Parker, and M. P. Allen (Kluwer, Dordrecht, 1990); M.J. Gillan, Philos. Mag. A **58**, 257 (1988).
[21] D.M. Ceperley, Rev. Mod. Phys. **67**, 279 (1995); **71**, S438 (1999).
[22] R. Ramírez and C.P. Herrero, Phys. Rev. B **48**, 14 659 (1993).
[23] J.C. Noya, C.P. Herrero, and R. Ramírez, Phys. Rev. B **53**, 9869 (1996).
[24] J.C. Noya, C.P. Herrero, and R. Ramírez, Phys. Rev. B **56**, 237 (1997).
[25] J. Tersoff, Phys. Rev. B **37**, 6991 (1988).
[26] J. Tersoff, Phys. Rev. B **39**, 5566 (1989); **41**, 3248(E) (1990).
[27] J. Tersoff, Phys. Rev. B **49**, 16 349 (1994).
[28] R. Ramírez and M. Böhm, J. Phys.: Condens. Matter **7**, 4847 (1995).
[29] R. Car and M. Parrinello, Phys. Rev. Lett. **55**, 2471 (1985).

[30] P.L. Silvestrelli, A. Alavi, M. Parrinello, and D. Frenkel, Phys. Rev. Lett. **77**, 3149 (1996); Phys. Rev. B **56**, 3806 (1997).
[31] N. Takeuchi, A. Selloni, and E. Tosatti, Phys. Rev. B **55**, 15 405 (1997).
[32] D. Marx and M. Parrinello, Nature (London) **375**, 216 (1995); Science **271**, 179 (1996).
[33] M. Benoit, D. Marx, and M. Parrinello, Nature (London) **392**, 258 (1998); D. Marx, M.E. Tuckerman, J. Hutter, and M. Parrinello, *ibid.* **397**, 601 (1999).
[34] G. P. Srivastava, *The Physics of Phonons* (Adam Hilger, Bristol, 1990).
[35] R. P. Feynman, *Statistical Mechanics* (Addison-Wesley, New York, 1972).
[36] N. W. Ashcroft and N. D. Mermin, *Solid State Physics* (Saunders College, Philadelphia, 1976).
[37] C. Kittel, *Introduction to Solid State Physics* (Wiley, New York, 1975).
[38] F.D. Murnaghan, Proc. Natl. Acad. Sci. U.S.A. **30**, 244 (1944).
[39] M.T. Yin and M.L. Cohen, Phys. Rev. B **26**, 5668 (1982).
[40] R. Biswas, R.M. Martin, R.J. Needs, and O.H. Nielsen, Phys. Rev. B **35**, 9559 (1987).
[41] *Physics of Group IV Elements and III-IV Compounds*, edited by O. Madelung, Landolt-Börnstein, New Series, Group III, Vol. 17, Pt. a (Springer-Verlag, Berlin, 1982).
[42] A.C. Victor, J. Chem. Phys. **36**, 1903 (1962).
[43] M.H. Müser, P. Nielaba, and K. Binder, Phys. Rev. B **51**, 2723 (1995).
[44] M.H. Grimsditch and A.K. Ramdas, Phys. Rev. B **11**, 3139 (1975).
[45] H.J. McSkimin and P. Andreatch, Jr., J. Appl. Phys. **43**, 2944 (1972).
[46] S. Fahy and S.G. Louie, Phys. Rev. B **36**, 3373 (1987).
[47] H. Holloway, K.C. Hass, M.A. Tamor, T.R. Anthony, and W.F. Banholzer, Phys. Rev. B **44**, 7123 (1991).
[48] T. Yamanaka, S. Morimoto, and H. Kanda, Phys. Rev. B **49**, 9341 (1994).
[49] A.K. Ramdas, S. Rodriguez, M. Grimsditch, T.R. Anthony, and W.F. Banholzer, Phys. Rev. Lett. **71**, 189 (1993).
[50] C.P. Herrero, Solid State Commun. **110**, 243 (1999).
[51] A. Debernardi and M. Cardona, Phys. Rev. B **54**, 11 305 (1996).
[52] G.A. Slack and S.F. Bartram, J. Appl. Phys. **46**, 89 (1975).